







































The First Habitable Zone Earth-Sized Planet From *TESS* II: *Spitzer* Confirms TOI-700 d

JOSEPH E. RODRIGUEZ ¹, ANDREW VANDERBURG ^{2, *}, SEBASTIAN ZIEBA ³, LAURA KREIDBERG ¹,
CAROLINE V. MORLEY ², JASON D. EASTMAN ¹, STEPHEN R. KANE ⁴, ALTON SPENCER⁵, SAMUEL N. QUINN ¹,
RYAN CLOUTIER ¹, CHELSEA X. HUANG ^{6, †}, KAREN A. COLLINS ¹, ANDREW W. MANN ⁷, EMILY GILBERT ^{8, 9, 10, 11},
JOSHUA E. SCHLIEDER^{10, 11}, ELISA V. QUINTANA ^{10, 11}, THOMAS BARCLAY ^{10, 12, 11}, GABRIELLE SUISSA ^{10, 11, 13},
RAVI KUMAR KOPPARAPU ^{10, 11, 14}, COURTNEY D. DRESSING ¹⁵, GEORGE R. RICKER⁶, ROLAND K. VANDERSPEK⁶,
DAVID W. LATHAM ¹, SARA SEAGER ^{6, 16, 17}, JOSHUA N. WINN ¹⁸, JON M. JENKINS ¹⁹, ZACHORY BERTA-THOMPSON ²⁰,
PATRICIA T. BOYD^{10, 11}, DAVID CHARBONNEAU ¹, DOUGLAS A. CALDWELL^{21, 19}, EUGENE CHIANG ¹⁵,
JESSIE L. CHRISTIANSEN ²², DAVID R. CIARDI ²², KNICOLE D. COLÓN ^{10, 11}, JOHN DOTY ²³, TIANJUN GAN ²⁴,
NATALIA GUERRERO ⁶, MAXIMILIAN N. GÜNTHER ^{6, †}, EVE J. LEE ²⁵, ALAN M. LEVINE ⁶, ERIC LOPEZ ^{10, 11},
PHILIP S. MUIRHEAD ²⁶, ELISABETH NEWTON²⁷, MARK E. ROSE ¹⁹, JOSEPH D. TWICKEN ^{21, 19}, JESUS NOEL VILLASEÑOR⁶

¹Center for Astrophysics | Harvard & Smithsonian, 60 Garden St, Cambridge, MA 02138, USA

²Department of Astronomy, The University of Texas at Austin, Austin, TX 78712, USA

³Universität Innsbruck, Institut für Astro- und Teilchenphysik, Technikerstraße 25, 6020 Innsbruck, Austria

⁴Department of Earth and Planetary Sciences, University of California, Riverside, CA 92521, USA

⁵Danbury High School, Danbury, CT 06811, USA

⁶Department of Physics and Kavli Institute for Astrophysics and Space Research, Massachusetts Institute of Technology, Cambridge, MA 02139, USA

⁷Department of Physics and Astronomy, University of North Carolina at Chapel Hill, Chapel Hill, NC 27599, USA

⁸Department of Astronomy and Astrophysics, University of Chicago, Chicago, IL 60637, USA

⁹The Adler Planetarium, 1300 South Lakeshore Drive, Chicago, IL 60605, USA

¹⁰Exoplanets and Stellar Astrophysics Laboratory, Code 667, NASA Goddard Space Flight Center, Greenbelt, MD 20771, USA

¹¹GSFC Sellers Exoplanet Environments Collaboration, NASA Goddard Space Flight Center, Greenbelt, MD 20771

¹²University of Maryland, Baltimore County, 1000 Hilltop Circle, Baltimore, MD 21250, USA

¹³Goddard Earth Sciences Technology and Research (GESTAR), Universities Space Research Association, Columbia, Maryland, USA

¹⁴NASA NExSS Virtual Planetary Laboratory, Box 951580, Seattle, WA 98195

¹⁵Department of Astronomy, University of California Berkeley, Berkeley, CA 94720-3411, USA

¹⁶Department of Earth, Atmospheric and Planetary Sciences, Massachusetts Institute of Technology, Cambridge, MA 02139, USA

¹⁷Department of Aeronautics and Astronautics, MIT, 77 Massachusetts Avenue, Cambridge, MA 02139, USA

¹⁸Department of Astrophysical Sciences, Princeton University, 4 Ivy Lane, Princeton, NJ, 08544, USA

¹⁹NASA Ames Research Center, Moffett Field, CA, 94035, USA

²⁰Department of Astrophysical and Planetary Sciences, University of Colorado, Boulder, CO 80309, USA

²¹SETI Institute, Mountain View, CA 94043, USA

²²Caltech/IPAC, 1200 E. California Blvd. Pasadena, CA 91125, USA

²³Noqsi Aerospace, Ltd., 15 Blanchard Avenue, Billerica, MA 01821, USA

²⁴Department of Astronomy and Tsinghua Centre for Astrophysics, Tsinghua University, Beijing 100084, China

²⁵Department of Physics and McGill Space Institute, McGill University, 3550 rue University, Montreal, QC, H3A 2T8, Canada

²⁶Department of Astronomy & Institute for Astrophysical Research, Boston University, 725 Commonwealth Avenue, Boston, MA 02215, USA

²⁷Department of Physics and Astronomy, Dartmouth College, Hanover, NH, USA

ABSTRACT

We present *Spitzer* 4.5 μ m observations of the transit of TOI-700 d, a habitable zone Earth-sized planet in a multiplanet system transiting a nearby M-dwarf star (TIC 150428135, 2MASS J06282325-6534456). TOI-700 d has a radius of $1.144^{+0.062}_{-0.061} R_{\oplus}$ and orbits within its host star's conservative habitable zone with a period of 37.42 days ($T_{\text{eq}} \sim 269$ K). TOI-700 also hosts two small inner planets ($R_b = 1.037^{+0.065}_{-0.064} R_{\oplus}$ & $R_c = 2.65^{+0.16}_{-0.15} R_{\oplus}$) with periods of 9.98 and 16.05 days, respectively. Our *Spitzer* observations confirm the *TESS* detection of TOI-700 d and remove any remaining doubt that it is a genuine planet. We analyze the *Spitzer* light curve combined

with the 11 sectors of *TESS* observations and a transit of TOI-700 c from the LCOGT network to determine the full system parameters. Although studying the atmosphere of TOI-700 d is not likely feasible with upcoming facilities, it may be possible to measure the mass of TOI-700 d using state-of-the-art radial velocity instruments (expected RV semi-amplitude of ~ 70 cm/s).

1. INTRODUCTION

Humans have wondered whether life exists elsewhere in the universe for centuries. Thanks to new technologies and rapid advancements in the study of exoplanets in the past few decades, we are making progress towards answering this question scientifically. So far, thousands of small exoplanets are known, most of which were discovered by the *Kepler* mission (Borucki et al. 2010) and astronomers have taken the first steps towards probing their compositions (e.g. Dressing et al. 2015; Rogers 2015) and atmospheres (e.g. Kreidberg et al. 2014). Now, more sensitive instruments (e.g. Szentgyorgyi et al. 2016) and telescopes (e.g. Gardner et al. 2006; Roberge & Moustakas 2018; Gaudi et al. 2018) are planned with the eventual goal of detecting biosignatures, in an Earth-like planetary atmosphere.

Though the possibility of detecting biosignatures in the future seems real, the prospects remain uncertain. Statistical results from *Kepler* have shown that small, habitable-zone planets are common around low-mass host stars (Dressing & Charbonneau 2015), but it is not clear how much these planets resemble the Earth. *Kepler* discovered potentially rocky habitable-zone planets around M-dwarf stars (Quintana et al. 2014), but they orbit stars too faint for precise radial velocity measurements, so we do not know if they are rocky like the Earth or if they are shrouded by thick atmospheres, inhospitable to life as we know it. Our best constraints on which planets are rocky and which have thick envelopes come from observations of highly-irradiated, hot planets (Rogers 2015; Wolfgang & Lopez 2015). So far, very few temperate planets that are similar to the size of the Earth orbit host stars bright enough to carry out precise mass measurements through radial velocities.

Learning more about small, temperate planets requires finding such planets around brighter stars. In April 2018, NASA’s Transiting Exoplanet Survey Satellite (*TESS*) mission launched with precisely this goal. So far, *TESS* has discovered over 1000 exoplanet candidates orbiting some of the brightest and closest stars to the Sun (Ricker et al. 2015, N. Guerrero et al. *in prep*). Most of these planets orbit close to their stars and have high equilibrium temperatures, which allow us to study planets in highly irradiated environments and probe atmospheric loss (e.g. Vanderspek et al. 2019; Kreidberg et al. 2019). *TESS* is also expected to discover a small number of planets in temperate orbits around low-mass M-

dwarf stars, possibly including rocky planets orbiting in their stars’ circumstellar habitable zones (Sullivan et al. 2015; Kaltenecker et al. 2019). Though *TESS* has detected slightly larger planets in temperate orbits (e.g. Günther et al. 2019) and terrestrial planets in hot orbits (e.g. Winters et al. 2019), so far no potentially rocky, habitable-zone planets have been reported.

In this paper, we confirm the first Earth-sized planet orbiting in its host star’s habitable zone discovered by *TESS*. The planet, TOI-700 d, is only $22\% \pm 7\%$ larger than Earth, orbits an M-dwarf star ($0.415 M_{\odot}$, TIC 150428135) located 31 parsecs from the Sun, and is a promising target for future observations to measure its mass. Unfortunately, atmospheric characterization will likely not be feasible with the James Webb Space Telescope (JWST, Beichman et al. 2014). In a companion to this paper, Gilbert et al. (2020) characterize the TOI-700 system and statistically validate TOI-700 d and two other planets in the system. TOI-700 d will likely be an attractive target for future observations, so independent confirmation of the planet’s existence is valuable before investing large amounts of telescope resources. Here, we present *Spitzer* Space Telescope observations that confirm TOI-700 d is a transiting planet and help to refine our knowledge of its parameters. Our paper is organized as follows: In §2 we discuss the *TESS* and *Spitzer* observations and reduction methods. We present our global analysis using EXOFASTv2 (Eastman et al. 2013, 2019) in §3. We place TOI-700 d in the context of presently known planets and examine future prospects for characterizing the planet’s mass and atmosphere in §4, and give our conclusions in §5.

2. OBSERVATIONS AND ARCHIVAL DATA

In this section we present the observations used to confirm the small habitable-zone planet TOI-700 d. In our analysis, we include the *TESS* discovery data and follow-up observations from *Spitzer* and the Las Cumbres Observatory (LCO). In the companion to this paper, Gilbert et al. (2020) characterized the TOI-700 system and validated the planets using a wealth of additional follow-up observations including multiple spectroscopic observations, high-spatial resolution speckle imaging, and ground-based time series photometry. An additional companion paper, Suissa et al. (2020), explored plausible atmospheres for TOI-700 d and the prospects for observing its atmosphere with future facilities. For brevity, we only describe the observations which directly feed into our EXOFASTv2 global analysis. See Table 1 for the literature magnitudes and kinematics.

* NASA Sagan Fellow

† Juan Carlos Torres Fellow

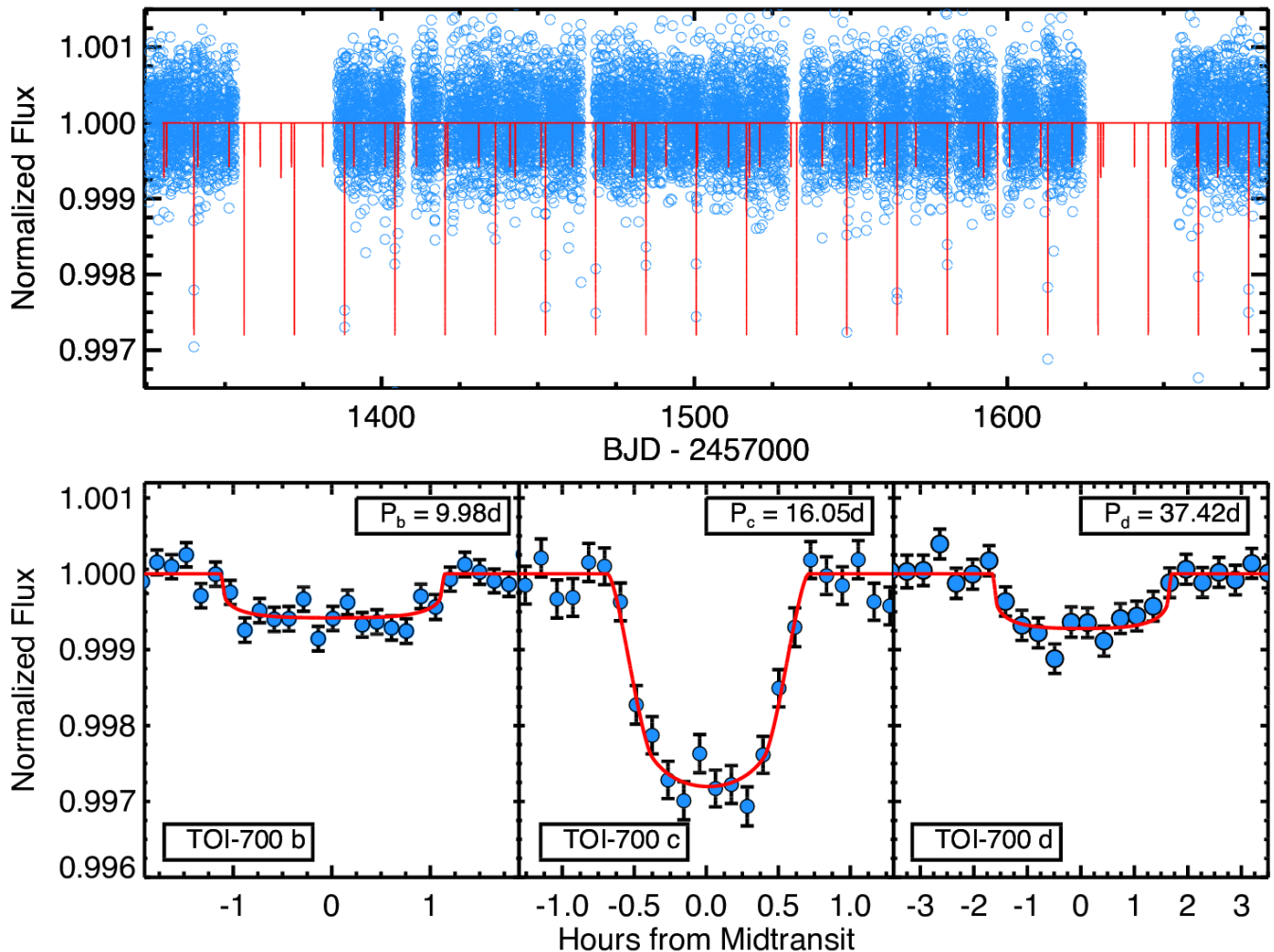


Figure 1. Photometric observations of the TOI-700 system. The light curve has been processed to remove stellar variability and instrumental systematics. *Top panel:* The blue open circles are the *TESS* observations binned to 30 minutes for all 11 sectors of *TESS*. Since TOI-700 falls near *TESS*'s continuous viewing zone, there are almost 10 months of data. *Bottom panels:* The *TESS* transits for (left) TOI-700 b, (middle) TOI-700 c, and (right) TOI-700 d phase folded to the best fit ephemeris from the global fit (see §3). The *TESS* observations have been binned for visual clarity. The EXOFASTv2 transit model is shown in red in each panel.

2.1. *TESS* Photometry

TESS observed TOI-700 between 25 July 2018 and 17 July 2019. Because TOI-700 is located near the southern ecliptic pole, it fell in a region of sky that was observed nearly continuously by *TESS*. In total, TOI-700 was observed during 11 *TESS* sectors. Though TOI-700 is a nearby, bright dwarf star, it was not originally pre-selected for high-cadence *TESS* observations because of incorrect catalog stellar parameters. It was, however, proposed as part of Guest Investigator proposal G011180 (PI Dressing), so pixel time series from a small region of the *TESS* CCD near TOI-700 were downlinked with two-minute sampling.

After the data were downlinked, they were reduced and analyzed by the Science Processing Operations Center (SPOC)

pipeline, based at the NASA Ames Research Center (Jenkins et al. 2016). The SPOC pipeline applies pixel-level calibrations to the data, identifies optimal photometric apertures, estimates flux contamination from other nearby stars, and extracts light curves. Instrumental artifacts are identified and removed from the light curves using the Presearch Data Conditioning (PDC) module (Smith et al. 2012; Stumpe et al. 2014). The processed light curves were searched for transits with the SPOC Transiting Planet Search (TPS, Jenkins 2002).

Early searches of the TOI-700 *TESS* light curves (both single sector and sectors 1-3) revealed some evidence for planetary transits, but these signals were not initially considered compelling enough to be promoted to the status of a planet candidate in the *TESS* Object of Interest (TOI) catalog (N.

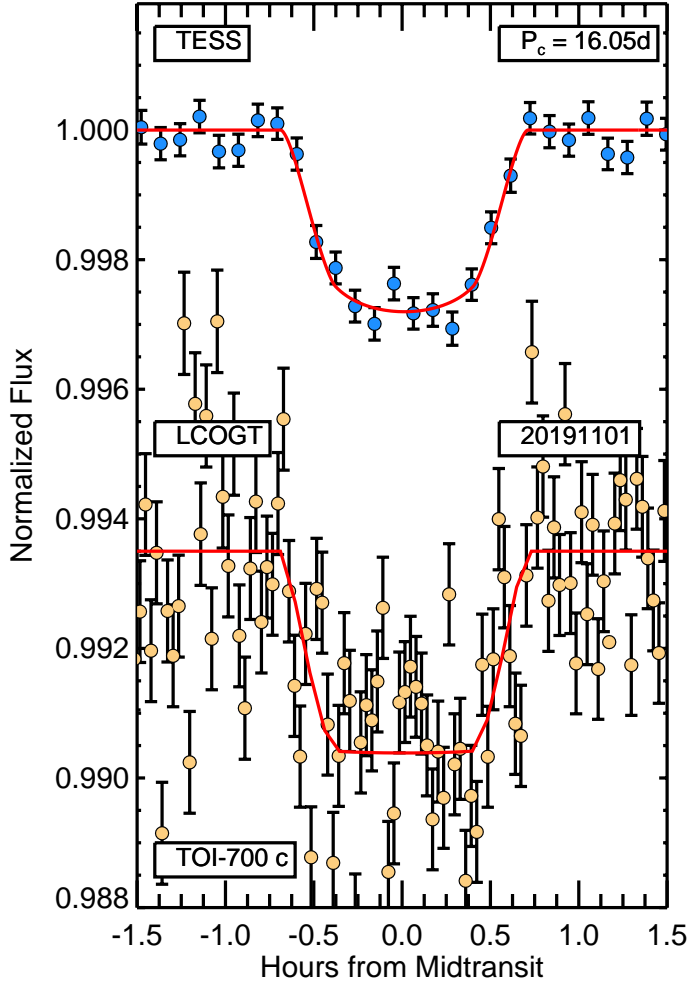


Figure 2. Photometric observations of the TOI-700 c from *TESS* and LCO (UT 2019 November 01). The *TESS* and LCO observations have been binned for visual clarity. The EXOFASTv2 transit model for each data set is shown in red for each observation.

Guerrero et al. *in prep*). After data from *TESS* sectors 1-6 were searched together, two planet candidates with 16.05 day and 37.42 day periods were detected and released in the online TOI catalog. A third planet candidate with period 9.98 days was detected in a subsequent search of data from *TESS* sectors 1-9, and a final search of the *TESS* full first-year dataset (11 sectors in total, see Figure 1) confirmed the detections (Twicken et al. 2018; Li et al. 2019).

These three candidates were investigated and characterized in detail by Gilbert et al. (2020), who statistically validated all three candidates as exoplanets. We note that it was more difficult to validate the planetary nature of the outer 37 day period planet candidate around TOI-700. The transit signal was detected by *TESS* on only 8 occasions and was fairly weak with a Multiple Event Statistic (MES, a proxy for signal-to-noise ratio used by the SPOC pipeline) of 9.3. Ex-

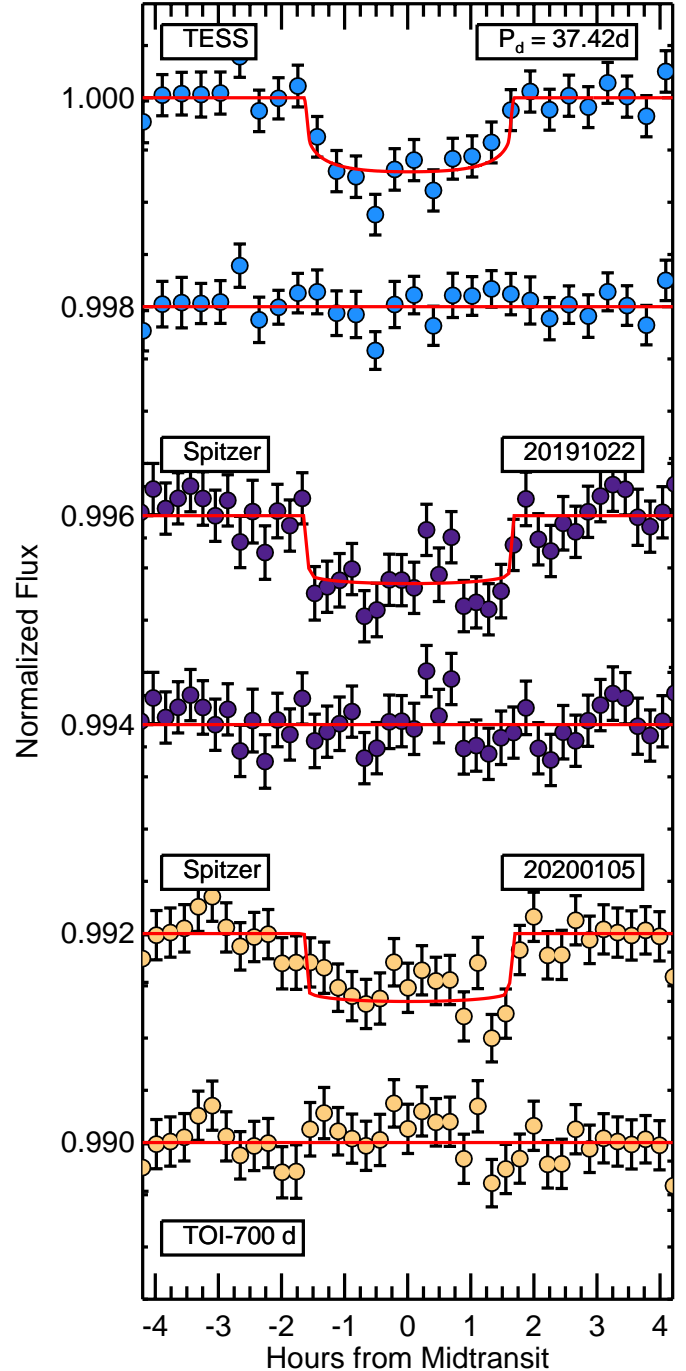


Figure 3. Photometric observations of the TOI-700 d from *TESS* and *Spitzer* (UT 2019 October 22 & UT 2020 January 05). The *TESS* and *Spitzer* observations have been binned for visual clarity. The EXOFASTv2 transit model for each data set is shown in red for each observation. The residuals of our model fit are shown below each lightcurve.

perience from the *Kepler* mission has shown that a significant fraction of planet candidates in the low signal-to-noise/few transit regime are false positives (Mullally et al. 2018; Burke

Table 1. Properties of TOI-700

Other identifiers			
TIC 150428135			
2MASS J06282325-6534456			
WISE J062823.05-653443.7			
Parameter	Description	Value	Source
α_{J2000}	Right Ascension (RA)	06:28:23.22878	1
δ_{J2000}	Declination (Dec)	-65:34:45.52157	1
l	Galactic Longitude	275.4682095°	1
b	Galactic Latitude	-26.8810581°	1
l	Ecliptic Longitude	275.4691°	1
b	Ecliptic Latitude	-26.8807°	1
G	Gaia G mag	12.0665±0.0005	1
J	2MASS J mag	9.469 ± 0.023	2
H	2MASS H mag	8.893 ± 0.027	2
K _S	2MASS K _S mag	8.634 ± 0.023	2
WISE1	WISE1 mag	8.511 ± 0.023	3
WISE2	WISE2 mag	8.387 ± 0.02	3
WISE3	WISE3 mag	8.289 ± 0.016	3
WISE4	WISE4 mag	8.267 ± 0.083	3
μ_{α}	Gaia DR2 proper motion in RA (mas yr ⁻¹)	-102.75 ± 0.05	1
μ_{δ}	Gaia DR2 proper motion in DEC (mas yr ⁻¹)	161.80 ± 0.06	1
π^{\ddagger}	Gaia Parallax (mas)	32.18 ± 0.0392 [†]	1
d	Distance (pc)	31.075±0.038 [‡]	1
Spec. Type	Spectral Type	M2V±1	4

NOTES: The uncertainties of the photometry have a systematic error floor applied.

[†] RA and Dec are in epoch J2000. The coordinates come from Vizier where the Gaia RA and Dec have been precessed to J2000 from epoch J2015.5.

[‡] Values have been corrected for the -0.82 μ as offset as advocated by [Stassun & Torres \(2018\)](#).

References are: ¹[Gaia Collaboration et al. \(2018\)](#), ²[Cutri et al. \(2003\)](#), ³[Cutri & et al. \(2014\)](#), ⁴[Gilbert et al. \(2020\)](#)

[et al. 2019](#)). Although [Gilbert et al. \(2020\)](#) showed that the false positive probability of TOI-700 d (including instrumental false alarms) was below the threshold required for statistical validation, a small possibility remained that TOI-700 d was spurious. Given the potential impact of the discovery, the likelihood that TOI-700 d will be the target of future observations, and the fact that we are still working to fully understand systematic errors in *TESS* data, we wanted an independent confirmation of the planet from another facility. We therefore proposed for observations with the *Spitzer* Space Telescope to confirm the planet by detecting a transit at the predicted time.

2.2. LCOGT Photometry of TOI-700 c

As part of the *TESS* Follow-up Observing Program (TFOP), a transit of TOI-700 c was observed on UT 2019

November 01 in the z' band using one of the 1.0m Las Cumbres Observatory Global Telescope Network (LCOGT) telescopes located at the South African Astronomical Observatory (SAAO) ([Brown et al. 2013](#))¹. The telescope is a Ritchey-Chretien Cassegrain with a 4k×4k Sinistro CCD with a 27' × 27' field-of-view and a 0.39'' pixel scale. The observations were scheduled using the *TESS* Transit Finder that is built from the *Tapir* software tool ([Jensen 2013](#)). The observations were reduced and the light curves were extracted using the *AstroImageJ* software package ([Collins et al. 2017](#)). The photometry was extracted using a 3.9'' aperture, as smaller apertures resulted in a significantly higher rms noise level. See Figure 2 for the plot of the LCOGT transit of TOI-700 c.

2.3. Spitzer Photometry of TOI-700 d

Two follow up transits of TOI-700 d were observed with the *Spitzer* InfraRed Array Camera (IRAC, [Fazio et al. 2004](#)) on UT 2019 October 22 and UT 2020 January 05 as part of a Director's Discretionary Time (DDT) proposal award (program number 14314, PI Vanderburg). Each observation was 8.9 hours in duration, with a two-second exposure time, and used Channel 2 on IRAC, which is equivalent to a photometric wavelength range of 4 – 5 μ m. Prior to the observations of TOI-700, a 30-minute burn-in sequence was conducted to allow the spacecraft to thermally equilibrate and the detector to asymptote to a steady state of charge trapping and release. For both the burn-in sequence and the time series observations, TOI-700 was placed on the detector on a pixel that is known to have minimal sensitivity variations.

We downloaded the *Spitzer* observations from the archive, and reduced the Basic Calibrated Data (BCD, provided by the *Spitzer* Science Center) using the custom aperture photometry routine developed by [Cubillos et al. \(2013\)](#). This analysis package (which is available open-source on GitHub²) fits a 2D Gaussian profile to the stellar image in each *Spitzer* exposure after upsampling by a factor of 5 in each spatial direction. We identified and masked pixels with outlying values using an iterative sigma-clipping procedure and then summed the flux in each fixed aperture. We tested apertures with radii ranging from 2 to 4 pixels in 0.25 pixel steps, and found that a radius of 3.0 pixels minimizes the noise in each of the extracted light curves. An annulus with an inner radius of 7 pixels and outer radius of 15 pixels was adopted for the determination of the median background value.

The dominating systematics for the 4.5 μ m *Spitzer* channel are intrapixel sensitivity variations ([Charbonneau et al. 2005](#)). We therefore fitted for them by using the BiLinearly-Interpolated Subpixel Sensitivity (BLISS) map technique in-

¹ <https://lco.global>

² <https://github.com/kevin218/POET>

roduced by [Stevenson et al. \(2012\)](#). We describe the full *Spitzer* light curve, $F(x, y, X, Y, t)$, by:

$$F(x, y, X, Y, t) = F_s R(t) M(x, y) T(t) G(X, Y, t), \quad (1)$$

where F_s is the constant out-of-transit flux, $R(t)$ is the ramp model, $M(x, y)$ is the BLISS map with (x, y) describing the position of the star on the detector, $T(t)$ is the [Mandel & Agol \(2002\)](#) transit model implemented in BATMAN ([Kreidberg 2015](#)) and $G(X, Y, t)$ is a term fitting for variations in the pixel response function (PRF) using a 2D cubic with the gaussian widths (X, Y) .

An initial fit with the BLISS map model revealed a clear transit in each of the *Spitzer* light curves with the same depth and duration seen in the *TESS* light curve. After detecting the transits, we adjusted our systematics correction to further optimize the *Spitzer* light curve. The optimal resolution for BLISS mapping was found to be 0.01 pixels for the first observation and 0.008 pixels for the second. We also experimented with the complexity of the light curve model. In order to compare models with different numbers of free parameters, we used the Bayesian Information Criterion (BIC, [Schwarz 1978](#), [Liddle 2007](#)). Combinations of a linear ramp $R(t)$ and PRF fits $G(X, Y, t)$ of different orders were tested. A significant increase in the BIC for those models showed that these more complex models are not justified.

Our final model consisted only of the BLISS map, a constant and the BATMAN transit model. The latter has the following parameters: T_0 , R_p/R_* , P , a/R_* , $\cos i$, e , ω_* , u_1 and u_2 (see [Table 2](#) for a description of these parameters). As multiple transits were observed with *TESS* and only two with *Spitzer*, we fixed the period P to the value determined by *TESS*.

Finally, we compared the *Spitzer* model with a fit which fixes the system specific parameters (P , a/R_* , $\cos i$) to values from a fit of the *TESS* observations only using EXOFASTv2. Both of these cases reproduce transit depths which are consistent with each other. The final fitted $4.5\mu\text{m}$ light curves from *Spitzer* with the EXOFASTv2 global model are shown in [Figure 3](#). *Spitzer* independently detected the transit of TOI-700 d with 12σ confidence.

In order to account for the correlated noise in our light curves, we calculate β , using the ‘‘time-averaging’’ method ([Pont et al. 2006](#); [Winn et al. 2007](#)). It scales the standard deviation of the data set with a factor β , which denotes the ratio between the actual achieved standard deviation of the binned residuals and the standard deviation in absence of red noise. By taking median values of this ratio for binnings between 15 and 30 minutes following [Winn et al. \(2008\)](#), we estimate $\beta_1 = 1.268$ for the first observation and $\beta_2 = 1.210$ for the second.

3. EXOFASTv2 GLOBAL FITS

To determine the full system parameters, and especially those of the habitable-zone Earth-sized planet, TOI-700 d, we globally fit the photometric observations from eleven sectors of *TESS*, the observations from *Spitzer*, and a follow up transit of TOI-700 c from the Las Cumbres Observatory using EXOFASTv2 ([Eastman et al. 2013, 2019](#)). We removed low-frequency variability from the *TESS* light curves by fitting the light curves with basis splines (with a 1.5 day knot spacing), ignoring points during the transits of the three planets, and iteratively excluding outliers (see [Fig. 3](#) from [Vanderburg & Johnson 2014](#)). For computational efficiency, we averaged the two-second cadence *Spitzer* light curve into one-minute bins. The *Spitzer* light curve had been corrected for systematics as described in [§2.3](#).

EXOFASTv2 models planetary systems self consistently, so the transit parameters of each planet, TOI-700 b, c, and d were fit simultaneously with, and informed by, their host star’s parameters. Because TOI-700 is a low-mass dwarf star, the stellar evolutionary and stellar atmospheric models embedded within EXOFASTv2 are not reliable. Therefore, we use the absolute K-mag relations from [Mann et al. \(2015, 2019\)](#) to determine the mass and radius of TOI-700, and use these values with a conservative 5% uncertainty as Gaussian priors on R_* and M_* of $0.419 \pm 0.021 R_\odot$ and $0.417 \pm 0.021 M_\odot$. We note that these values are well within 1σ of the mass and radius used for TOI-700 from [Gilbert et al. \(2020\)](#). We do not use the [Claret \(2017\)](#) limb-darkening tables within the global fit to constrain u_1 and u_2 , and instead leave the limb-darkening parameters to be constrained by the transit light curves in each bandpass, as well as EXOFASTv2’s built in uniform prior that only allows steps within the physical bounds identified by [Kipping \(2013\)](#) for any band: $u_1 + u_2 < 1$, $u_1 > 0$, and $u_1 + 2u_2 > 0$. We also place priors on T_{eff} (3460 ± 65 K) and $[\text{Fe}/\text{H}]$ (-0.07 ± 0.11 dex) from an analysis of spectroscopic observations using the Southern Astrophysical Research (SOAR) Telescope combined with an spectral energy distribution analysis (see [Gilbert et al. \(2020\)](#)). Since priors are placed on M_* and R_* , the corresponding priors on T_{eff} and $[\text{Fe}/\text{H}]$ do not affect the fitted planet parameters, and are only used to derive quantities such as L_* and T_{eq} , along with the predicted *Spitzer* 3.6 and $4.5\mu\text{m}$ eclipse depths shown in [Table 2](#). To account for the possible correlated noise in the *Spitzer* observations, we have modified the per point error for each *Spitzer* light curve following [Winn et al. \(2008\)](#). Specifically, the per point errors on for the *Spitzer* light curves are derived by multiplying the β parameter calculated for each *Spitzer* light curve (see [§2.3](#)) and the light curve rms. See [Figures 1, 2, and 3](#) light curve plots of the *TESS*, LCOGT, *Spitzer* with the EXOFASTv2 models (light curves are available with this publication).

Since we are simultaneously modeling photometric data for TOI-700 d from different observatories, we performed

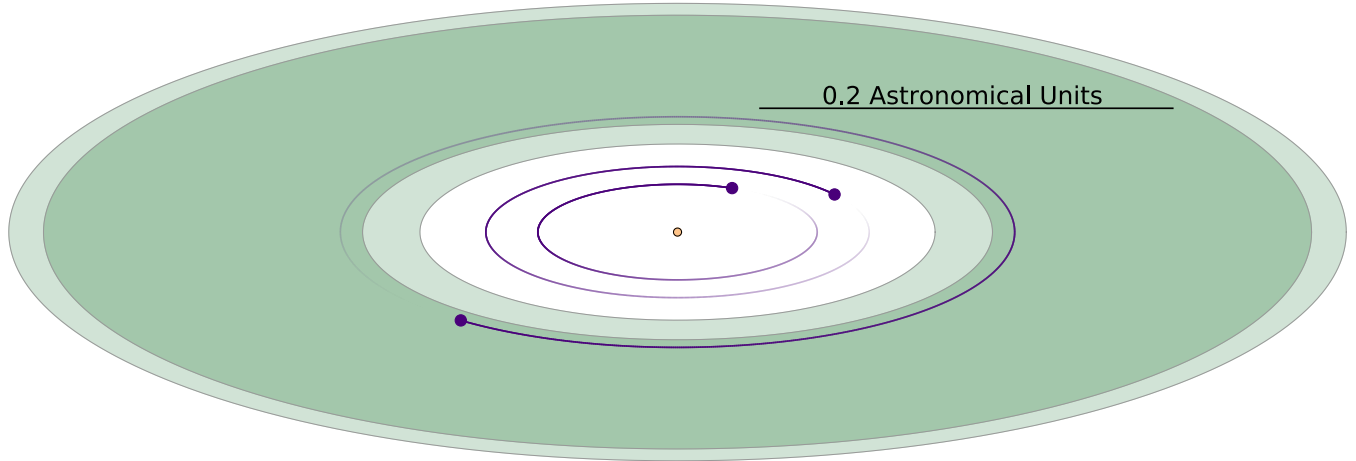


Figure 4. Schematic of the TOI-700 system, from the vantage of an observer inclined by 20 degrees from the plane of the system, showing the orbits of the planets (faded purple lines), the conservative habitable zone (dark green), and the optimistic extension to the habitable zone (light green, [Kasting et al. 1993](#); [Kane & Gelino 2012](#); [Kopparapu et al. 2013, 2014](#)). The size of the star TOI-700 is shown to scale, but the sizes of the planets are not.

some experiments to ensure that the data from *TESS* and *Spitzer* were consistent and neither significantly biased the transit depth. We do not perform these tests on the LCOGT observations because the LCOGT observations are far less precise. We tested the *TESS* and *Spitzer* datasets for consistency by jointly fitting the two light curves, allowing for a dilution term in either data set while using the other as the baseline for comparison. Fitting for a dilution term in one bandpass effectively decoupled the measured transit depth from the two observatories. In all cases, the fit results were consistent with no significant additional dilution needed – in other words, the transit depth measured by *TESS* was consistent with that measured by *Spitzer*. This is not surprising given that the SPOC pipeline accounts for blending from nearby stars in the *TESS* data and that none of our follow up observations, including the *Spitzer* images and high spatial resolution speckle observations, show evidence of any unknown additional stellar companions close enough to contaminate the *Spitzer* photometry.

4. DISCUSSION

TOI-700 is a compelling system for future characterization observations thanks to its relative proximity ($d=31.075\pm 0.038$ pc) and brightness ($H = 8.893 \pm 0.027$). All three planets orbiting TOI-700 are sub-Neptune in size ($R_b = 1.037^{+0.065}_{-0.064} R_{\oplus}$, $R_c = 2.65^{+0.16}_{-0.15} R_{\oplus}$, and $R_d = 1.144^{+0.062}_{-0.061} R_{\oplus}$), and orbit with periods of 9.977, 16.0511, and 37.425 days. We note that the ratio of planet’s orbital periods is 1.608 for c:b, and the d:c ratio is 2.33. These ratios are within 1% of an 8:5 resonance c:b and 7:3 for d:c. See Section 6.3 of [Gilbert et al. \(2020\)](#) which presents a detailed transit timing and photodynamical analysis. Their results suggest minimal perturbations on the orbit of planet d from planets b and c. We see no evidence of transit timing

variations in the combined *Spitzer* and *TESS* global fit, supporting their result. We also see a slight mid-transit brightening during the *Spitzer* observations of TOI-700 d. However, since it is similar in amplitude to other features in the light curve, not seen in the *TESS* observations, and that there is correlated noise in the *Spitzer* data, we do not believe it to be astrophysical in origin. We direct the reader to [Gilbert et al. \(2020\)](#) for a detailed analysis and discussion of the TOI-700 system as a whole (and the validation of all three planets in the system), and we focus the rest of our discussion on TOI-700 d, the first habitable-zone Earth-sized planet from NASA’s *TESS* mission.

4.1. *Spitzer* Confirmation of TOI-700 d

While [Gilbert et al. \(2020\)](#) were able to rule out most false positive scenarios for TOI-700 d, a small probability remained that the planet was not real. Our *Spitzer* observations rule out many of the remaining false positive scenarios for the planet candidate. Most importantly, we have now detected TOI-700 d’s transit with two different telescopes, so systematic errors in the *TESS* light curve cannot be the source of the signal. Given TOI-700 d’s relatively low detection significance and small number of observed transits, instrumental artifacts were the greatest uncertainty in the validation of TOI-700 d. The *Spitzer* observations have retired this risk.

Spitzer also showed that the transit of TOI-700 d is achromatic, which constrains blended companions and rejects additional astrophysical false positive scenarios. We measured the transit depths (R_p^2/R_*^2) in the *TESS* and *Spitzer* bandpasses by fitting the light curves simultaneously with [Mandel & Agol \(2002\)](#) models using an affine invariant Markov Chain Monte Carlo sampler ([Goodman & Weare 2010](#)). We found that the *Spitzer* transit (612 ± 44 ppm) is slightly shallower than the *TESS* signal (677 ± 98 ppm). We constrained

Table 2. Median values and 68% confidence interval for global model of TOI-700

Parameter	Description (Units)	Values			
Stellar Parameters:					
M_*	Mass (M_\odot)	0.415 ± 0.020			
R_*	Radius (R_\odot)	0.424 ± 0.017			
L_*	Luminosity (L_\odot)	0.0232 ^{+0.0027} _{-0.0025}			
ρ_*	Density (cgs)	7.68 ^{+1.0} _{-0.89}			
log g	Surface gravity (cgs)	4.80 ^{+0.038} _{-0.039}			
T_{eff}	Effective Temperature (K)	3461 ± 66			
[Fe/H]	Metallicity (dex)	−0.07 ± 0.11			
Planetary Parameters:					
		b	c	d	
P	Period (days)	9.97702 ^{+0.00024} _{-0.00028}	16.051110 ^{+0.000062} _{-0.000063}	37.42475 ^{+0.00036} _{-0.00040}	
R_P	Radius (R_\oplus)	1.037 ^{+0.065} _{-0.064}	2.65 ^{+0.16} _{-0.15}	1.144 ^{+0.062} _{-0.061}	
T_C	Time of conjunction (BJD _{TDB})	2458331.3537 ^{+0.00059} _{-0.00032}	2458340.08813 ± 0.00095	2458330.4754 ^{+0.00047} _{-0.00041}	
T_0^\dagger	Optimal conjunction Time (BJD _{TDB})	2458490.9867 ^{+0.00027} _{-0.00029}	2458548.75256 ± 0.00050	2458742.1476 ^{+0.00016} _{-0.00012}	
a	Semi-major axis (AU)	0.0677 ± 0.0011	0.0929 ± 0.0015	0.1633 ^{+0.0026} _{-0.0027}	
i	Inclination (Degrees)	89.66 ^{+0.24} _{-0.29}	88.868 ^{+0.083} _{-0.10}	89.79 ^{+0.14} _{-0.12}	
e	Eccentricity	0.081 ^{+0.095} _{-0.058}	0.078 ^{+0.075} _{-0.056}	0.111 ^{+0.14} _{-0.078}	
ω_*	Argument of Periastron (Degrees)	−75 ⁺⁹⁴ ₋₈₄	81 ⁺⁸⁰ ₋₈₃	0 ⁺¹⁴⁰ ₋₁₃₀	
T_{eq}	Equilibrium temperature (K)	417 ± 12	356 ± 10.	268.8 ^{+7.7} _{-7.6}	
R_P/R_*	Radius of planet in stellar radii	0.0224 ^{+0.0010} _{-0.0011}	0.0573 ^{+0.0020} _{-0.0018}	0.02476 ^{+0.00088} _{-0.00089}	
a/R_*	Semi-major axis in stellar radii	34.3 ^{+1.5} _{-1.4}	47.1 ^{+2.0} _{-1.9}	82.9 ^{+3.5} _{-3.3}	
δ	Transit depth (fraction)	0.000503 ^{+0.000048} _{-0.000046}	0.00329 ^{+0.00024} _{-0.00020}	0.000613 ^{+0.000045} _{-0.000043}	
$Depth$	Flux decrement at mid transit	0.000503 ^{+0.000048} _{-0.000046}	0.00329 ^{+0.00024} _{-0.00020}	0.000613 ^{+0.000045} _{-0.000043}	
τ	Ingress/egress transit duration (days)	0.00220 ^{+0.00029} _{-0.00017}	0.0138 ^{+0.0026} _{-0.0023}	0.00367 ^{+0.00078} _{-0.00032}	
T_{14}	Total transit duration (days)	0.0943 ^{+0.0056} _{-0.0049}	0.0589 ^{+0.0019} _{-0.0018}	0.1384 ^{+0.0033} _{-0.0027}	
T_{FWHM}	FWHM transit duration (days)	0.0920 ^{+0.0055} _{-0.0048}	0.0451 ^{+0.0020} _{-0.0023}	0.1345 ^{+0.0031} _{-0.0027}	
b	Transit Impact parameter	0.21 ^{+0.19} _{-0.15}	0.893 ^{+0.017} _{-0.021}	0.30 ^{+0.19} _{-0.20}	
b_S	Eclipse impact parameter	0.20 ^{+0.15} _{-0.14}	0.951 ^{+0.14} _{-0.074}	0.30 ^{+0.12} _{-0.19}	
τ_S	Ingress/egress eclipse duration (days)	0.00205 ± 0.00023	0.0141 ^{+0.0078} _{-0.014}	0.00366 ^{+0.00041} _{-0.00038}	
$T_{S,14}$	Total eclipse duration (days)	0.0888 ^{+0.0075} _{-0.0095}	0.052 ^{+0.011} _{-0.052}	0.138 ^{+0.015} _{-0.016}	
$T_{S,FWHM}$	FWHM eclipse duration (days)	0.0867 ^{+0.0074} _{-0.0093}	0.026 ^{+0.023} _{-0.026}	0.134 ^{+0.015} _{-0.016}	
$\delta_{S,3.6\mu m}$	Blackbody eclipse depth at 3.6 μm (ppm)	0.068 ^{+0.020} _{-0.017}	0.085 ^{+0.031} _{-0.024}	0.00039 ^{+0.00019} _{-0.00013}	
$\delta_{S,4.5\mu m}$	Blackbody eclipse depth at 4.5 μm (ppm)	0.358 ^{+0.085} _{-0.072}	0.63 ^{+0.18} _{-0.14}	0.0063 ^{+0.0024} _{-0.0018}	
$\langle F \rangle$	Incident Flux ($10^9 \text{ erg s}^{-1} \text{ cm}^{-2}$)	0.00681 ^{+0.00083} _{-0.00077}	0.00362 ^{+0.00043} _{-0.00039}	0.00116 ^{+0.00014} _{-0.00013}	
T_P	Time of Periastron (BJD _{TDB})	2458327.3 ^{+3.1} _{-2.8}	2458324.0 ^{+3.3} _{-3.1}	2458297 ⁺¹⁰ ₋₁₂	
T_S	Time of eclipse (BJD _{TDB})	2458326.36 ^{+0.49} _{-0.51}	2458332.07 ^{+0.73} _{-0.68}	2458311.8 ^{+3.3} _{-3.2}	
T_A	Time of Ascending Node (BJD _{TDB})	2458328.80 ^{+0.23} _{-0.44}	2458336.23 ^{+0.56} _{-0.34}	2458321.1 ^{+1.7} _{-2.1}	
T_D	Time of Descending Node (BJD _{TDB})	2458333.90 ^{+0.44} _{-0.24}	2458343.96 ^{+0.55} _{-0.55}	2458339.8 ^{+2.1} _{-1.7}	
$e \cos \omega_*$		−0.000 ^{+0.078} _{-0.080}	0.000 ^{+0.071} _{-0.067}	0.00 ± 0.14	
$e \sin \omega_*$		−0.027 ^{+0.043} _{-0.085}	0.031 ^{+0.077} _{-0.044}	−0.001 ^{+0.056} _{-0.086}	
$M_P \sin i$	Minimum mass (M_\oplus)	1.25 ^{+1.00} _{-0.35}	7.9 ^{+2.7} _{-1.8}	1.94 ^{+0.69} _{-0.57}	
M_P/M_*	Mass ratio	0.0000091 ^{+0.0000073} _{-0.0000025}	0.000057 ^{+0.000020} _{-0.000013}	0.0000140 ^{+0.0000051} _{-0.0000041}	
d/R_*	Separation at mid transit	35.1 ^{+3.3} _{-2.5}	45.3 ^{+3.6} _{-4.3}	82.2 ^{+7.9} _{-7.6}	
Wavelength Parameters:					
		z'	4.5 μm	TESS	
u_1	linear limb-darkening coeff	0.36 ^{+0.36} _{-0.25}	0.128 ^{+0.19} _{-0.095}	0.20 ^{+0.12} _{-0.11}	
u_2	quadratic limb-darkening coeff	0.02 ^{+0.31} _{-0.26}	0.08 ^{+0.24} _{-0.14}	0.48 ± 0.13	
A_D	Dilution from neighboring stars	–	–	−0.000 ± 0.011	
Transit Parameters:					
		TESS	Spitzer UT 20191022 (4.5 μm)	LCO SAAO UT 20191101 (z')	Spitzer UT 20200105 (4.5 μm)
σ^2	Added Variance	0.000000091 ^{+0.000000036} _{-0.000000035}	0.000000050 ^{+0.000000082} _{-0.000000038}	0.00000266 ^{+0.00000042} _{-0.00000037}	0.0000000048 ^{+0.000000079} _{-0.000000036}
F_0	Baseline flux	1.000072 ^{+0.000017} _{-0.000016}	1.000063 ^{+0.000040} _{-0.000041}	0.99989 ± 0.00017	1.000078 ^{+0.000041} _{-0.000040}

NOTES: See Table 3 in Eastman et al. (2019) for the definition and explanation of the derived and fitted parameters in EXOFASTv2.

Equilibrium temperature is calculated assuming zero albedo and perfect heat redistribution: $T_{\text{eq}} = T_{\text{eff}} \sqrt{\frac{R_*}{2a}}$

The derived secondary eclipse depths assume a Bond albedo of zero.

[†]Minimum covariance with period.

All values in this table for the secondary occultation of TOI-700 b are predicted values from our global analysis.

red contaminants by comparing the measured ratio of the *Spitzer/TESS* depths ($0.90^{+0.14}_{-0.12}$) to the expected ratios for a variety of cooler companions using Equation 5 from Désert et al. (2015) and MIST isochrones (Choi et al. 2016). We rule out blends with very red, co-moving stars with mass less than $0.30 M_{\odot}$ (95% confidence). The *Spitzer* observations eliminate almost all remaining false positive scenarios for TOI-700 d, especially instrumental artifacts. These data, combined with the observations and statistical validation presented by Gilbert et al. (2020), allow us to confidently pursue future observations.

4.2. *Spitzer* Improvement on TOI-700 c and d’s Parameters

From our joint *TESS* and *Spitzer* global fit, we are able to improve the properties of TOI-700 d, relative to the results of an EXOFASTv2 fit that only included the *TESS* observations. This is similar to the fit that is presented in Gilbert et al. (2020), except they used the *exoplanet* software package (Foreman-Mackey & Barentsen 2019). This comparison removes any concern that any observed differences or improvements are caused by the analysis methodology. The *Spitzer* observations took place on UT 2019 October 22 and UT 2020 January 05, 99 and 174 days after the end of the 11 *TESS* sectors in which TOI-700 was observed (UT 2019 July 17), extending the total time baseline of observations by 49%. The combined *Spitzer* transits are detected at $\sim 14\sigma$ while the *TESS* combined transits are detected at 7σ . This expansion in the photometric baseline yielded a 61% improvement on the average precision on TOI-700 d’s orbital period. Additionally, thanks to its infrared capability (ideal for M-dwarfs like TOI-700) and larger aperture compared to *TESS*, *Spitzer* was able to reduce the uncertainty in R_p/R_* for TOI-700 d’s by 39%. Our analysis also included a transit of TOI-700 c from LCOGT on UT 2019 November 01, 108 days after the end of the 11 sectors of *TESS*. Our analysis shows a 32% improvement on the precision of TOI-700 c’s orbital period and a 9% improvement on the planet’s R_p/R_* .

The improved precision of these parameters will pay dividends as more follow-up observations of TOI-700 d are conducted. The improved orbital period measurement will help plan future transit observations of TOI-700 d more efficiently, and our more precise radius measurement will be critical for understanding the planet’s bulk composition. Decreasing radius uncertainties is particularly important for understanding the composition of rocky planets. For rocky planets (with some constant bulk iron/silicate abundance ratio), the planet’s mass m and radius r are related by $m \propto r^{3.6}$ (Zeng et al. 2016). This means that when inferring a rocky planet’s iron/silicate ratio, a planet’s radius must be known 3.6 times more precisely than its mass for the two observables to contribute equally. In other words, improving the radius precision will improve the ability of future radial ve-

locity observations to determine TOI-700 d’s bulk composition.

4.3. TOI-700’s Habitable Zone

The location of the habitable zone of planetary systems is calculated based on the premise that a planet similar to Earth could retain surface liquid water given sufficient atmospheric pressure (Kasting et al. 1993; Kane & Gelino 2012; Kopparapu et al. 2013, 2014). Such calculations are sensitive to the precision of the stellar parameters (Kane 2014, 2018); in particular the luminosity and effective temperature of the host star. Specifically, the habitable-zone boundaries are estimated using 1-dimensional cloud-free climate models that monitor the change in surface radiative balance for an Earth analog as a function of incident flux at infrared wavelengths. For this purpose, we utilize equations 4 and 5 along with the coefficients of table 1 from Kopparapu et al. (2014) to calculate the habitable-zone boundaries. The habitable zone is often described as either “conservative” with boundaries of runaway greenhouse and maximum greenhouse, or “optimistic” with boundaries determined from empirical assumptions of water prevalence on Venus and Mars (Kane et al. 2016). We use the stellar parameters shown in Table 2 to calculate the extent of the TOI-700 habitable zone for both the conservative and optimistic cases. Figure 4 shows a schematic of the TOI-700 system comparing the orbits of the planets to the location of the conservative and optimistic habitable zones. TOI-700 d’s orbit lies confidently within the conservative habitable zone, and is small enough (only 20% larger than the Earth) that it could be terrestrial (Rogers 2015; Wolfgang & Lopez 2015). It is worth noting the caveat that there are various effects that influence the boundaries of the habitable zone. In the case of tidal locking, calculations from climate models have demonstrated that this generally has the effect of widening the habitable zone (Yang et al. 2013, 2019). Based on estimates of tidal locking time scales by Barnes (2017), the majority of habitable-zone terrestrial planets discovered by *TESS* are expected to be tidally locked for ages less than ~ 1 Gyr, therefore increasing the confidence in the habitable-zone status of TOI-700 d.

4.4. Known habitable-zone Terrestrial-Sized Planets

TOI-700 d joins a very small population of presently-known habitable-zone terrestrial-sized planets. In this subsection, we compare TOI-700 d to a sample of habitable-zone planets very similar in size to the Earth. Starting from a list of known small habitable-zone planets³, we identify planets smaller than $1.5 R_{\oplus}$, the radius below which hot planets orbiting M-dwarfs similar to TOI-700 ($0.415 \pm 0.021 M_{\odot}$) tend to have rocky compositions (Rogers 2015; Fulton et al.

³ <http://phl.upr.edu/projects/habitable-exoplanets-catalog>

2017; Cloutier & Menou 2019). After this cut, we are left with ten small habitable-zone⁴ planets: TRAPPIST-1 (d, e, f, & g; Gillon et al. 2017), *Kepler*-186 f (Quintana et al. 2014), *Kepler*-1229 b (Morton et al. 2016), *Kepler*-442 b (Torres et al. 2015), *Kepler*-62 f (Borucki et al. 2013), *Kepler*-1649 c (Vanderburg et al. 2020) (this was recently announced and not in the known list at the time of this paper), and TOI-700 d. We note that this cut removes all RV only planets and LHS-1140 b ($1.73 R_{\oplus}$), which has a density consistent with a rocky composition (Dittmann et al. 2017; Ment et al. 2019). Of the remaining planets, TOI-700 d orbits the brightest host star by far. In the optical, TOI-700’s *Gaia* G-band magnitude (12.07) is 4.5 times brighter than the next brightest host (*Kepler*-62, $G = 13.72$), and in the near-infrared, TOI-700’s K-band magnitude (8.63) is 4.6 times brighter than the next brightest host (TRAPPIST-1, $K = 10.30$). TOI-700’s apparent brightness makes it particularly attractive among small habitable-zone planets for follow-up observations.

4.5. Future Radial Velocity Observations of TOI-700 d

Among small, habitable-zone planets, TOI-700 d is well-suited for precise radial velocity observations to measure its mass and confirm/rule out a rocky composition. Its host star is a quiet M-dwarf ($0.415 M_{\odot}$) with no large photometric variations observed in the full *TESS* light curve. The host star appears to be relatively inactive with a long rotation period of 54 ± 0.8 days. With no signs of activity in the spectra and a rotation period that differs from the orbital period, TOI-700 should be well suited for RV follow up (we direct the reader to Gilbert et al. (2020) for a thorough discussion on the stellar classification, including spectral analysis). Using the Chen & Kipping (2017) mass/radius relation⁵, our EXOFASTv2 model reports mass estimates for TOI-700 b, c, and d to be $M_b = 1.25^{+1.00}_{-0.35} M_{\oplus}$, $M_c = 7.9^{+2.7}_{-1.8} M_{\oplus}$, and $M_d = 1.94^{+0.69}_{-0.57} M_{\oplus}$, which correspond to radial velocity semi-amplitudes of $0.67^{+0.54}_{-0.19}$, $3.61^{+1.3}_{-0.82}$, and $0.68^{+0.24}_{-0.20} \text{ m s}^{-1}$. Figure 5 compares the radial velocity accessibility of TOI-700 d to other known transiting exoplanets. The symbol size is inversely proportional to a simple metric estimating the amount of observing time required to detect each planet’s RV signal (assuming the Weiss & Marcy 2014 mass/radius relation):

$$\text{Point Size} \propto K^2 \times 10^{-0.4G} \quad (2)$$

Where K is the semi-amplitude and G is the *Gaia* G-band magnitude of the host star. By this metric, TOI-700 d is the best small habitable-zone (conservative) planet ($R_p < 1.5 R_{\oplus}$) for RV observations. Detecting the RV signal of TOI-

700 d will be challenging, but is within the current capabilities of the most precise spectrographs like the Echelle Spectrograph for Rocky Exoplanets and Stable Spectroscopic Observations (ESPRESSO) on the VLT (Pepe et al. 2010). ESPRESSO is stable enough to detect the planet’s $\approx 80 \text{ cm s}^{-1}$ signal and TOI-700 is bright enough that ESPRESSO should achieve $\approx 70 \text{ cm s}^{-1}$ photon-limited precision in 1-hour exposures (Pepe et al. 2014; Faria et al. 2019, and private communication).

4.6. Future Atmospheric Characterization of TOI-700 d

Despite its favorable properties, TOI-700 d will be a challenging target for transit spectroscopy observations to search for biosignatures or other molecules in its atmosphere in the near future. To assess the feasibility of detecting these features, we simulated JWST spectra for the planet (assuming Earth-like and CO_2 dominated atmospheres) with Pandexo (Batalha et al. 2017) using the NIRSpec/G235M observing mode. This mode provides the highest signal-to-noise for the transmission spectra of rocky planets around M-dwarfs (Morley et al. 2017). Assuming photon noise limited observations, distinguishing such features from a featureless spectrum at 5σ confidence would require data spanning more than 200 transits ($\gtrsim 1000$ hours), equivalent to observing every single transit of TOI-700 d for the first 20 years after JWST’s launch. It would also require an order of magnitude higher precision on the transit depth measurements than has ever been achieved (Line et al. 2016). TOI-700 d requires significantly more observing time than the TRAPPIST-1 planets because of the relatively small planet-to-star radius ratio. We direct the reader to paper III in this series that does a much more in depth analysis of TOI-700 d’s possible atmosphere, including a 3-D general circulation model of plausible atmospheres and their detectability using future observatories (Sussisa et al. 2020). While follow-up JWST observations are not practical, the discovery of this planet motivates the development of future large-aperture observing facilities capable of sub-10 ppm measurement precision in the near-infrared.

5. CONCLUSION

We present new *Spitzer* observations confirming the planetary nature of the TOI-700 d, a habitable-zone Earth-sized planet located within a multiplanet system. TOI-700 is a early M-dwarf ($M_{\star} = 0.415 \pm 0.020 M_{\odot}$ and $R_{\star} = 0.424 \pm 0.017 R_{\odot}$) located 31.1 pc from the Sun. Using a combination of high spatial resolution speckle imaging, spectroscopic observations from CHIRON, and ground-based seeing limited photometry from the TESS Followup Observing Program (TFOP), (Gilbert et al. 2020) were able to statistically validate the planetary nature of TOI-700 b, c, and d. Although the calculated false positive probability was low enough for the planet to be statistically validated, we sought

⁴ K2-72 e and TRAPPIST-1 d orbit in their star’s optimistic habitable zones, while the others orbit within the conservative habitable zone.

⁵ If we adopt the Weiss & Marcy (2014) mass-radius relation, we get similar masses for each planet: $M_b = 1.1 M_{\oplus}$, $M_c = 6.7 M_{\oplus}$, and $M_d = 2.2 M_{\oplus}$.

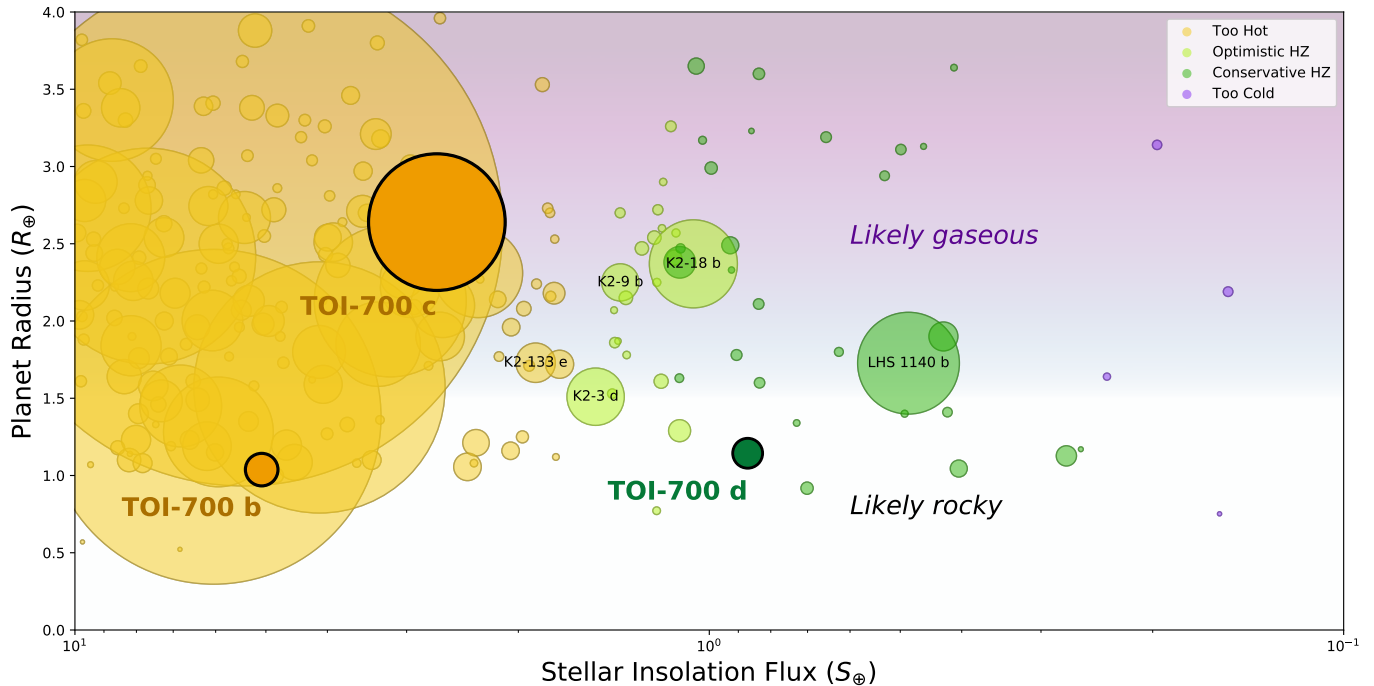


Figure 5. TOI-700 in the context of known exoplanets. Using data from the NASA Exoplanet Archive (Akeson et al. 2013), we plot the radius of known exoplanets versus the incident flux they receive from their host stars. The symbols are color coded based on their position relative to the circumstellar habitable zone, where yellow dots represent planets too hot to have liquid water, purple dots represent planets too cold to have liquid water, and light and dark green points represent planets in the optimistic and conservative habitable zones, respectively. The background shading indicates whether a planet is likely rocky or gaseous based on its size alone, following (Rogers 2015; Wolfgang & Lopez 2015). We used the polynomial expressions from Kopparapu et al. (2014) to determine the boundaries of the optimistic and conservative habitable zones for each host star. The area of the symbol is inversely proportional to the amount of observing time required to measure the planet’s mass with radial velocity observations – larger points are easier measurements (see §4.5). In terms of RV accessibility, TOI-700 d stands out as one of the best habitable-zone planets with a radii small enough that they are likely rocky. We note that LHS 1140 b is more accessible based on our metrics and has a measured mass consistent with it being rocky (Dittmann et al. 2017; Ment et al. 2019).

independent transit confirmation with *Spitzer* given the importance of the discovery and the relatively low S/N of the transit signal from *TESS*. Our $4.5\mu\text{m}$ *Spitzer* observations conclusively confirmed the transit of TOI-700 d, ruling out any remaining instrumental origin for the signal and solidifying its validation.

We model the *TESS* and *Spitzer* photometry to determine the full system parameters. TOI-700 hosts two Earth-sized planets and a sub-Neptune ($R_b = 1.044^{+0.065}_{-0.063} R_{\oplus}$, $R_c = 2.64^{+0.16}_{-0.14} R_{\oplus}$, and $R_d = 1.220^{+0.073}_{-0.063} R_{\oplus}$) with periods of $P_b = 9.97702^{+0.00024}_{-0.00028}$ days, $P_c = 16.051108^{+0.000062}_{-0.000064}$ days, and $P_d = 37.42469^{+0.00033}_{-0.00042}$ days. TOI-700 d is located well within the conservative habitable zone for its host star, and is the first habitable-zone Earth-sized planet discovered from NASA’s *TESS* mission. TOI-700 is the brightest known host of a transiting habitable-zone Earth-sized planet discovered to date.

Although atmospheric characterization is likely out of reach of current and upcoming facilities, TOI-700 d provides a rare opportunity to measure the planet’s mass with state of the art facilities like ESPRESSO on the VLT (Pepe et al. 2010). Future observations should focus on measuring the mass of all three planets to gain insight into whether or not

Earth-sized planets around low-mass stars are similar to the Earth. The *TESS* mission was recently selected for its first extended mission, which will begin in the summer of 2020. According to the draft observing schedule, TOI-700 will be observed in 11 more sectors during *TESS* cycle 3⁶ providing a great opportunity to refine the ephemerides and parameters of the three known planets, and possibly detect additional planets in the system that would enhance our understanding of TOI-700’s architecture.

⁶ <https://heasarc.gsfc.nasa.gov/cgi-bin/tess/webtess/wtv.py>

ACKNOWLEDGMENTS

AV's work was performed under contract with the California Institute of Technology (Caltech)/Jet Propulsion Laboratory (JPL) funded by NASA through the Sagan Fellowship Program executed by the NASA Exoplanet Science Institute. MNG acknowledges support from MIT's Kavli Institute as a Juan Carlos Torres Fellow. CDD acknowledges support from the NASA TESS Guest Investigator Program through Grant 80NSSC18K1583. EDL is thankful for support from GSFC Sellers Exoplanet Environments Collaboration (SEEC), which is funded by the NASA Planetary Science Divisions Internal Scientist Funding Model. JNW thanks the Heising-Simons Foundation for support. EAG thanks the LSSTC Data Science Fellowship Program, which is funded by LSSTC, NSF Cybertraining Grant #1829740, the Brinson Foundation, and the Moore Foundation; her participation in the program has benefited this work. EAG is thankful for support from GSFC Sellers Exoplanet Environments Collaboration (SEEC), which is funded by the NASA Planetary Science Division's Internal Scientist Funding Model.

This work is based on observations made with the *Spitzer* Space Telescope, which is operated by the Jet Propulsion Laboratory, California Institute of Technology under a contract with NASA. Support for this work was provided by NASA through an award issued by JPL/Caltech. This research has made use of SAO/NASA's Astrophysics Data System Bibliographic Services. This research has made use of the SIMBAD database, operated at CDS, Strasbourg, France. This work has made use of data from the Eu-

ropean Space Agency (ESA) mission *Gaia* (<https://www.cosmos.esa.int/gaia>), processed by the *Gaia* Data Processing and Analysis Consortium (DPAC, <https://www.cosmos.esa.int/web/gaia/dpac/consortium>). Funding for the DPAC has been provided by national institutions, in particular the institutions participating in the *Gaia* Multilateral Agreement. This work makes use of observations from the Las Cumbres Observatory Global Telescope Network. We thank Kevin Stevenson for making the POET pipeline open-source and freely available on GitHub.

Funding for the *TESS* mission is provided by NASA's Science Mission directorate. We acknowledge the use of public *TESS* Alert data from pipelines at the *TESS* Science Office and at the *TESS* Science Processing Operations Center. This research has made use of the NASA Exoplanet Archive and the Exoplanet Follow-up Observation Program website, which are operated by the California Institute of Technology, under contract with the National Aeronautics and Space Administration under the Exoplanet Exploration Program. This paper includes data collected by the *TESS* mission, which are publicly available from the Mikulski Archive for Space Telescopes (MAST). This paper includes observations obtained under Gemini program GN-2018B-LP-101. Resources supporting this work were provided by the NASA High-End Computing (HEC) Program through the NASA Advanced Supercomputing (NAS) Division at Ames Research Center for the production of the SPOC data products.

Software: EXOFASTv2 (Eastman et al. 2013, 2019), AstroImageJ (Collins et al. 2017), BATMAN (Kreidberg 2015), Forecaster (Chen & Kipping 2017)

Facilities: TESS, Spitzer, LCOGT, Gaia, MAST

REFERENCES

- Akeson, R. L., Chen, X., Ciardi, D., et al. 2013, *PASP*, 125, 989
- Barnes, R. 2017, *Celestial Mechanics and Dynamical Astronomy*, 129, 509
- Batalha, N. E., Kempton, E. M.-R., & Mbarek, R. 2017, *ArXiv e-prints*, arXiv:1701.00012
- Beichman, C., Benneke, B., Knutson, H., et al. 2014, *PASP*, 126, 1134
- Borucki, W. J., Koch, D., Basri, G., et al. 2010, *Science*, 327, 977
- Borucki, W. J., Agol, E., Fressin, F., et al. 2013, *Science*, 340, 587
- Brown, T. M., Baliber, N., Bianco, F. B., et al. 2013, *PASP*, 125, 1031
- Burke, C. J., Mullally, F., Thompson, S. E., Coughlin, J. L., & Rowe, J. F. 2019, *AJ*, 157, 143
- Charbonneau, D., Allen, L. E., Megeath, S. T., et al. 2005, *ApJ*, 626, 523
- Chen, J., & Kipping, D. 2017, *ApJ*, 834, 17
- Choi, J., Dotter, A., Conroy, C., et al. 2016, *ApJ*, 823, 102
- Claret, A. 2017, *A&A*, 600, A30
- Cloutier, R., & Menou, K. 2019, *arXiv e-prints*, arXiv:1912.02170
- Collins, K. A., Kielkopf, J. F., Stassun, K. G., & Hessman, F. V. 2017, *AJ*, 153, 77
- Cubillos, P., Harrington, J., Madhusudhan, N., et al. 2013, *ApJ*, 768, 42
- Cutri, R. M., & et al. 2014, *VizieR Online Data Catalog*, 2328, 0
- Cutri, R. M., Skrutskie, M. F., van Dyk, S., et al. 2003, *VizieR Online Data Catalog*, 2246, 0
- Désert, J.-M., Charbonneau, D., Torres, G., et al. 2015, *ApJ*, 804, 59
- Dittmann, J. A., Irwin, J. M., Charbonneau, D., et al. 2017, *Nature*, 544, 333
- Dressing, C. D., & Charbonneau, D. 2015, *ApJ*, 807, 45
- Dressing, C. D., Charbonneau, D., Dumusque, X., et al. 2015, *ApJ*, 800, 135

- Eastman, J., Gaudi, B. S., & Agol, E. 2013, *PASP*, 125, 83
- Eastman, J. D., Rodriguez, J. E., Agol, E., et al. 2019, arXiv e-prints, arXiv:1907.09480
- Faria, J. P., Adibekyan, V., Amazo-Gómez, E. M., et al. 2019, arXiv e-prints, arXiv:1911.11714
- Fazio, G. G., Hora, J. L., Allen, L. E., et al. 2004, *ApJS*, 154, 10
- Foreman-Mackey, D., & Barentsen, G. 2019, *dfm/exoplanet: exoplanet v0.1.3*, doi:10.5281/zenodo.2536576
- Fulton, B. J., Petigura, E. A., Howard, A. W., et al. 2017, *AJ*, 154, 109
- Gaia Collaboration, Brown, A. G. A., Vallenari, A., et al. 2018, *A&A*, 616, A1
- Gardner, J. P., Mather, J. C., Clampin, M., et al. 2006, *SSRv*, 123, 485
- Gaudi, B. S., Seager, S., Mennesson, B., et al. 2018, *Nature Astronomy*, 2, 600
- Gilbert, E. A., Barclay, T., Schlieder, J. E., et al. 2020, arXiv e-prints, arXiv:2001.00952
- Gillon, M., Triaud, A. H. M. J., Demory, B.-O., et al. 2017, *Nature*, 542, 456
- Goodman, J., & Weare, J. 2010, *Communications in Applied Mathematics and Computational Science*, Vol. 5, No. 1, p. 65-80, 2010, 5, 65
- Günther, M. N., Pozuelos, F. J., Dittmann, J. A., et al. 2019, *Nature Astronomy*, 420
- Jenkins, J. M. 2002, *ApJ*, 575, 493
- Jenkins, J. M., Twicken, J. D., McCauliff, S., et al. 2016, in *Proc. SPIE*, Vol. 9913, *Software and Cyberinfrastructure for Astronomy IV*, 99133E
- Jensen, E. 2013, *Tapir: A web interface for transit/eclipse observability*, *Astrophysics Source Code Library*, ascl:1306.007
- Kaltenegger, L., Pepper, J., Stassun, K., & Oelkers, R. 2019, *ApJL*, 874, L8
- Kane, S. R. 2014, *ApJ*, 782, 111
- . 2018, *ApJL*, 861, L21
- Kane, S. R., & Gelino, D. M. 2012, *PASP*, 124, 323
- Kane, S. R., Hill, M. L., Kasting, J. F., et al. 2016, *ApJ*, 830, 1
- Kasting, J. F., Whitmire, D. P., & Reynolds, R. T. 1993, *Icarus*, 101, 108
- Kipping, D. M. 2013, *MNRAS*, 435, 2152
- Kopparapu, R. K., Ramirez, R. M., SchottelKotte, J., et al. 2014, *ApJL*, 787, L29
- Kopparapu, R. K., Ramirez, R., Kasting, J. F., et al. 2013, *ApJ*, 765, 131
- Kreidberg, L. 2015, *PASP*, 127, 1161
- Kreidberg, L., Bean, J. L., Désert, J.-M., et al. 2014, *Nature*, 505, 69
- Kreidberg, L., Koll, D. D. B., Morley, C., et al. 2019, *Nature*, 573, 87
- Li, J., Tenenbaum, P., Twicken, J. D., et al. 2019, *PASP*, 131, 024506
- Liddle, A. R. 2007, *MNRAS*, 377, L74
- Line, M. R., Stevenson, K. B., Bean, J., et al. 2016, *AJ*, 152, 203
- Mandel, K., & Agol, E. 2002, *ApJL*, 580, L171
- Mann, A. W., Feiden, G. A., Gaidos, E., Boyajian, T., & von Braun, K. 2015, *ApJ*, 804, 64
- Mann, A. W., Dupuy, T., Kraus, A. L., et al. 2019, *ApJ*, 871, 63
- Ment, K., Dittmann, J. A., Astudillo-Defru, N., et al. 2019, *AJ*, 157, 32
- Morley, C. V., Kreidberg, L., Rustamkulov, Z., Robinson, T., & Fortney, J. J. 2017, *ApJ*, 850, 121
- Morton, T. D., Bryson, S. T., Coughlin, J. L., et al. 2016, *ApJ*, 822, 86
- Mullally, F., Thompson, S. E., Coughlin, J. L., Burke, C. J., & Rowe, J. F. 2018, *AJ*, 155, 210
- Pepe, F., Molaro, P., Cristiani, S., et al. 2014, arXiv e-prints, arXiv:1401.5918
- Pepe, F. A., Cristiani, S., Rebolo Lopez, R., et al. 2010, *Society of Photo-Optical Instrumentation Engineers (SPIE) Conference Series*, Vol. 7735, *ESPRESSO: the Echelle spectrograph for rocky exoplanets and stable spectroscopic observations*, 77350F
- Pont, F., Zucker, S., & Queloz, D. 2006, *MNRAS*, 373, 231
- Quintana, E. V., Barclay, T., Raymond, S. N., et al. 2014, *Science*, 344, 277
- Ricker, G. R., Winn, J. N., Vanderspek, R., et al. 2015, *Journal of Astronomical Telescopes, Instruments, and Systems*, 1, 014003
- Roberge, A., & Moustakas, L. A. 2018, *Nature Astronomy*, 2, 605
- Rogers, L. A. 2015, *ApJ*, 801, 41
- Schwarz, G. 1978, *Annals of Statistics*, 6, 461
- Smith, J. C., Stumpe, M. C., Van Cleve, J. E., et al. 2012, *PASP*, 124, 1000
- Stassun, K. G., & Torres, G. 2018, *ApJ*, 862, 61
- Stevenson, K. B., Harrington, J., Fortney, J. J., et al. 2012, *ApJ*, 754, 136
- Stumpe, M. C., Smith, J. C., Catanzarite, J. H., et al. 2014, *PASP*, 126, 100
- Suissa, G., Wolf, E. T., Kopparapu, R. k., et al. 2020, arXiv e-prints, arXiv:2001.00955
- Sullivan, P. W., Winn, J. N., Berta-Thompson, Z. K., et al. 2015, *ApJ*, 809, 77
- Szentgyorgyi, A., Baldwin, D., Barnes, S., et al. 2016, *Society of Photo-Optical Instrumentation Engineers (SPIE) Conference Series*, Vol. 9908, *The GMT-Consortium Large Earth Finder (G-CLEF): an optical Echelle spectrograph for the Giant Magellan Telescope (GMT)*, 990822
- Torres, G., Kipping, D. M., Fressin, F., et al. 2015, *ApJ*, 800, 99
- Twicken, J. D., Catanzarite, J. H., Clarke, B. D., et al. 2018, *PASP*, 130, 064502
- Vanderburg, A., & Johnson, J. A. 2014, *PASP*, 126, 948

- Vanderburg, A., Rowden, P., Bryson, S., et al. 2020, ApJL, 893, L27
- Vanderspek, R., Huang, C. X., Vanderburg, A., et al. 2019, ApJL, 871, L24
- Weiss, L. M., & Marcy, G. W. 2014, ApJL, 783, L6
- Winn, J. N., Holman, M. J., Bakos, G. Á., et al. 2007, AJ, 134, 1707
- Winn, J. N., Holman, M. J., Torres, G., et al. 2008, ApJ, 683, 1076
- Winters, J. G., Medina, A. A., Irwin, J. M., et al. 2019, AJ, 158, 152
- Wolfgang, A., & Lopez, E. 2015, ApJ, 806, 183
- Yang, J., Abbot, D. S., Koll, D. D. B., Hu, Y., & Showman, A. P. 2019, ApJ, 871, 29
- Yang, J., Cowan, N. B., & Abbot, D. S. 2013, ApJL, 771, L45
- Zeng, L., Sasselov, D. D., & Jacobsen, S. B. 2016, ApJ, 819, 127